Scientific council of Faculty of Electrical Engineering and Information Technology

Slovak University of Technology in Bratislava

Ing. Boris Brunner

MgB_2 Wires Made by Diffusion Method and Their Properties

Summary of doctoral dissertation

A dissertation submitted for the degree of Philosophiae Doctor in doctoral study programme:
5.2.48 Physical Engineering

Bratislava 2016

This thesis was developed in a full-time doctoral study at Institute of Electrical Engineering, Slovak Academy of Sciences in Bratislava.

Author: Ing. Boris Brunner
IEE SAS, Dúbravská cesta 9, 74104 Bratislava

Supervisor: Ing. Pavol Kováč, DrSc.
IEE SAS, Dúbravská cesta 9, 74104 Bratislava

Opponents: .....
.....
.....

.....
.....
.....

Thesis summary was submitted on .....

Date of PhD thesis defence .....
Committee for dissertation defence in the doctoral study programme is appointed by chairman of joint study programme committee on .....
Code of programme: 5.2.48, doctoral study programme: Physical Engineering

Chairman of joint study programme committee: .....

Content

1 Introduction

This dissertation thesis deals with properties of MgB_2 wires produced by the diffusion method (internal Mg diffusion-IMD) and compares them with MgB_2 wires produced by different technological processes or with other superconducting materials (pnictide Sr-122). The aim of the thesis was the production process optimization in terms of electrical qualities of MgB_2 wires. For this purpose several kinds of powder precursors and dopants were processed under varying conditions. Subsequently, superconducting and microstructure properties like transition temperature, critical current density, pinning energies, phase composition, grain connectivity, were studied on the wire samples.

The first two chapters of the thesis give an overview of main features of superconducting materials, their categorization and a description of how they interact with magnetic field. The next chapter is dedicated to MgB_2, its basic microstructural and physical properties as well as to the production methods. The fourth and fifth chapter deal with the theory underlying phenomena occurring in superconductors and experimental techniques used to investigate them, respectively. The following five chapters contain original results of author´s research. The thesis closes with the conclusions and findings.

2 Description of the analysed conductors

To date, the most common fabrication method of MgB_2 superconducting wires has been the powder-in-tube process (PIT) with either the in-situ [1, 2] or ex-situ route [3, 4]. In order to eliminate or limit the issues linked to the PIT process, such as low superconductor density, void formation and high core porosity due to volume shrinking during sintering, Giunchi *et al.* [5] proposed a method called reactive liquid-Mg infiltration process which is often referred to as internal Mg diffusion (IMD) process. Based on the diffusion of metallic Mg into B powder, the method yields typical hollow MgB_2 wires.

2.1 In-situ and ex-situ powder-in-tube method

The most favourite and convenient production method of MgB_2 wires is the powder-in-tube (PIT) process. For its simplicity it is frequently used and considered one of the most effective and economic production methods of MgB_2. The procedure is simple and its schema is shown in Figure 1.

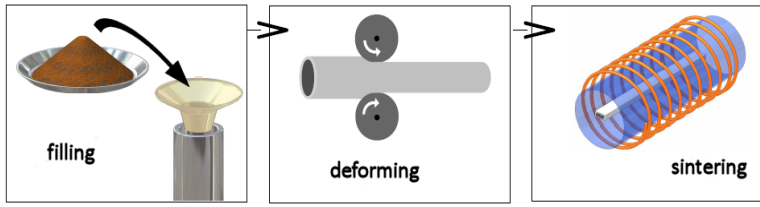

Figure 1 Powder-in-tube process steps

The PIT process has two routes: in-situ or ex-situ PIT. In-situ PIT sinters the Mg and B stoichiometric powder mixture, the ex-situ PIT process uses already pre-reacted MgB_2 powder which is packed into a metal tube, the tube deformed to a wire and heat-treated (Figure 2). Cross section of a wire produced by the in-situ PIT process can be seen in Figure 3.

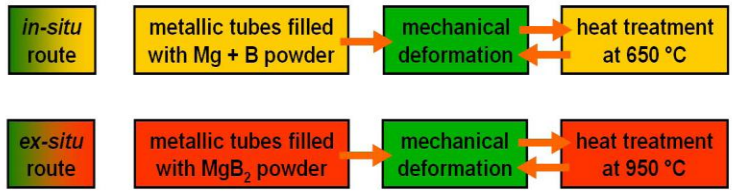

Figure 2 In-situ and ex-situ powder-in-tube process

After filling the powder into a metal tube, the tube has to be deformed to a wire. Deformation is usually done using a combination of several techniques like rotary swaging, two-axial rolling and groove rolling. Rotary swaging is an important step for powder densification. The level of densification depends on powder morphology and the strength of the tube material. Rotary swaging is typically followed by two-axial rolling and groove rolling. This kind of deformation has the advantage of symmetrical pressure distribution in the material of the arising wire.

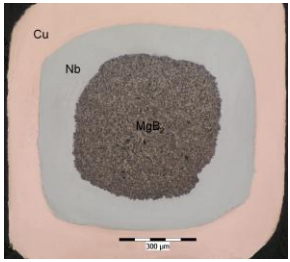

Figure 3 Cross section of MgB_2/Nb/Cu wire produced by the in-situ PIT process

When the desired wire dimension is reached, the wire is sintered at a temperature around 650°C. As it comes to volume reduction during sintering, the PIT method is distinguished by high superconductor porosity and thus consequently insufficient current carrying capability in the superconducting core.

2.2 Internal magnesium diffusion method

In order to avoid the drawbacks of the PIT process, Giunchi came up with a method based on the diffusion of magnesium into boron powder called internal magnesium diffusion (IMD) to manufacture typical hollow MgB_2 wires. Unlike PIT, which reacts solely powders, this technique uses a metallic magnesium rod and boron powder. The process starts with a composite consisting of an outer metallic sheath containing a central rod of pure Mg surrounded by B powder, which is cold-worked to a wire. The steps of the process are schematically shown in Figure 4.

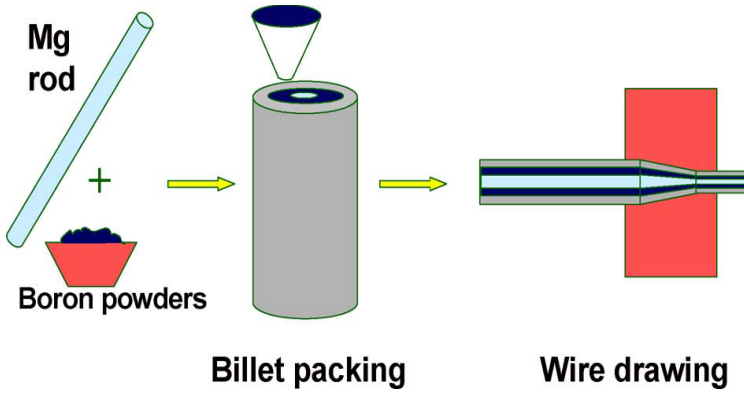

Figure 4 Steps of the IMD process

When a Mg rod is placed at the center of a metal tube, the space between the rod and the inner wall of the tube is filled with boron powder. Subsequently, the filled powder is densified by hand-pressing with a steel tube of appropriate size and by rotary swaging of the composite. This is followed by either two-axial rolling or by groove rolling.

During heat-treatment at a temperature around the melting point of Mg (650°C), Mg diffuses into boron powder (hence the name internal Mg diffusion-IMD) and a high density MgB_2 of great phase purity is formed. The diffusion reaction results in an annular MgB_2 layer (Figure 5) with a hole in the place where Mg rod was.

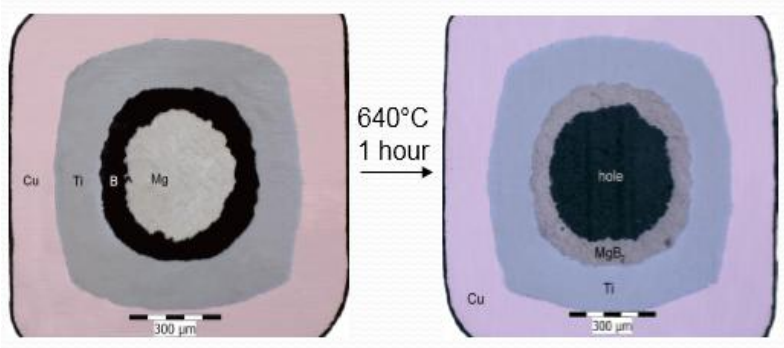

Figure 5 Cross section of a MgB_2 wire produced by the IMD technique before and after heat-treatment at 640°C for 1 hour

For the purpose of examining the properties of wires in more detail, the modified IMD technique was developed (MIMD), enabling production of MgB_2 cores which are extractable from their metallic sheath. For this reason most of the wires presented in this thesis had been prepared using MIMD technique. The MIMD process uses a Mg tube filled with B powder, which is embedded in a metallic sheath. Such assembled composite is deformed to a wire and heat-treated to create a cylindrical MgB_2 core (Figure 6). Since the original IMD process results in wires with hollow brittle MgB_2 filament, it is practically impossible to extract the filament and examine features like grain connectivity and phase purity. Therefore, the MIMD procedure was employed, yielding cylindrical MgB_2 cores allowing detailed investigation of superconductor properties.

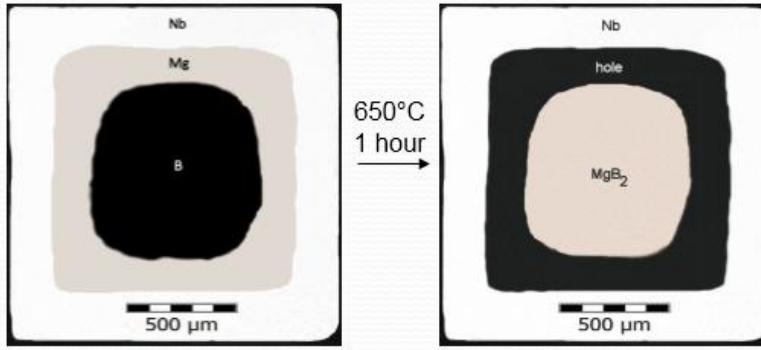

Figure 6 Cross section of a MgB_2 wire produced by MIMD technique before and after heat-treatment at 650°C for 1 hour

3 Experimental

The main measurement instrument was the Model 6000 Physical Property Measurement System (PPMS) made by Quantum Design, Inc. In this work the vibrating sample magnetometer (VSM) option of the PPMS was used to determine the transition temperature T_c, the critical current density J_c and the mean effective activation energy of flux lines U.

The critical temperature (T_c) of the samples and the width of their superconducting transition (ΔT_c) were determined from the temperature dependence of magnetic moment (Figure 7). T_c was determined from the ZFC curve as the temperature corresponding to the first point deviating from the zero moment line, or in other words, by the onset of diamagnetism. ΔT_c was determined by the 10-90% criterion, as the difference $T_{90\%} - T_{10\%}$.

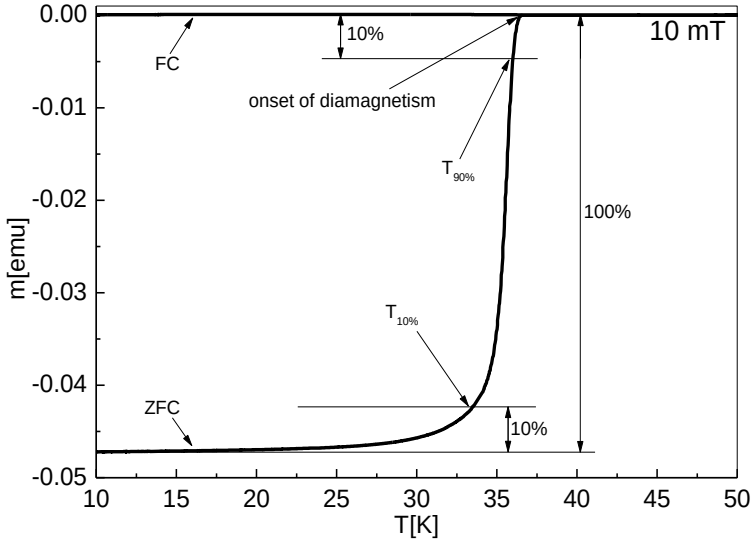

Figure 7 Typical $m(T)$-curve measured at 10 mT with indicated onset of diamagnetism corresponding to the transition temperature and $T_{90\%}$ and $T_{10\%}$, used to determine the width of the transition as their difference. ZFC and FC refer to the zero field cooled and field cooled curve, respectively.

To determine the critical current density J_c of the samples, the field dependence of magnetic moment $m(B)$ was measured. The samples were cooled down to the measuring temperature from above T_c in zero magnetic field. Hysteresis loops were recorded between -2 T and 14 T with a constant field sweep of 6.3 mT/s in the temperature range 4.2 K-32 K in 2 K steps. The field was directed parallel and perpendicular to the wire axis. Examples of hysteresis loops measured at three different temperatures are shown in Figure 8. The critical current density was determined from the loops by using Bean's critical state model to establish

a relationship between the width of the hysteresis loop Δm and the critical current density.

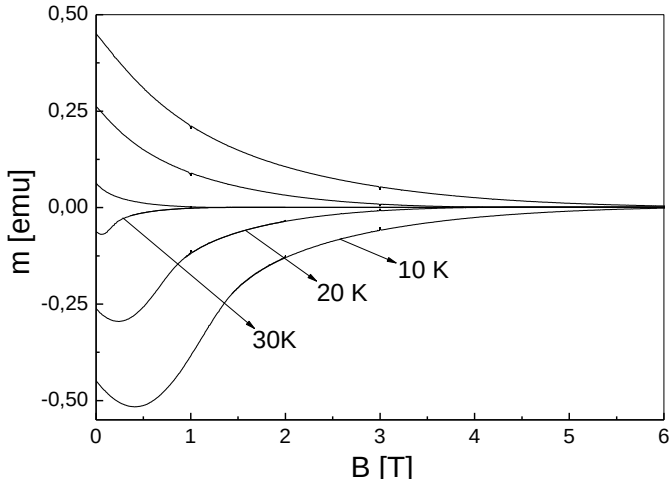

Figure 8 Examples of hysteresis loops measured at 10 K, 20 K and 30 K.

During hysteresis loop measurements the field sweep was interrupted at selected fields and the time dependence of irreversible magnetic moment was measured. Examples of the thus obtained relaxation curves at various temperatures can be seen in Figure 9.

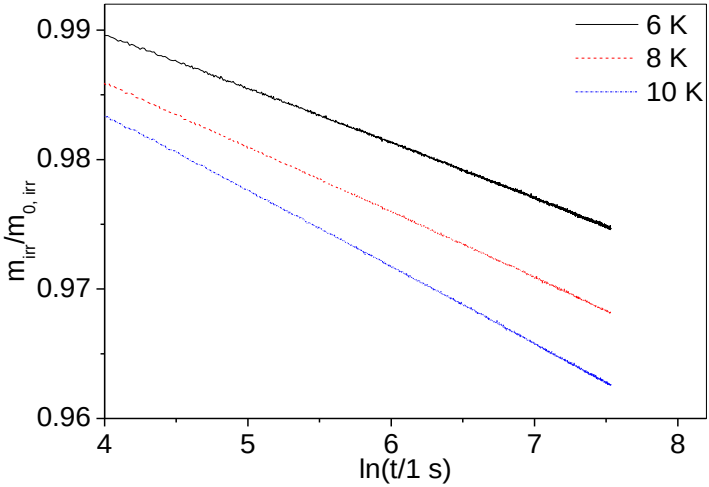

Figure 9 Examples of relaxation curves at various temperatures

From these relaxation curves the mean effective activation energy of flux lines was calculated within the Anderson`s flux creep theory [6], where the time dependence of irreversible magnetization is in first approximation logarithmic and given by

$$M(t,T) = M_0(T)\left[1 - \frac{k_B T}{U(T)} ln\left(1 + \frac{t_b}{\tau}\right)\right]$$

with $M_0(T)$ the magnetization at the beginning of the relaxation taken as t_b = 60 s and τ the intrinsic relaxation time assumed to be in the interval 10^{-12} s $< \tau < 10^{-6}$ s. By introducing the normalized flux creep rate S as the slope of the curves in Figure 9 divided by the initial value of magnetization at t_b

$$S = \frac{1}{M_0}\frac{dM}{dlnt}$$

and by combining it with equation for the magnetization, one gets for the mean effective pinning energy $U(T)$

$$\frac{1}{S} + 17{,}9 \leq \frac{U(T)}{k_B T} \leq \frac{1}{S} + 31{,}7$$

4 Results

4.1 Superconducting and structural properties of wires produced by the internal Mg diffusion method and powder-in-tube process

Mono-core MgB_2 wires produced by the in-situ powder-in-tube (PIT) technique and internal magnesium diffusion (IMD) were investigated. For the PIT wire, a Mg powder of purity 99.8% (particles size ~43μm) and a B powder of purity 99% (particles size ~200 nm) weighed in stoichiometric ratio were mixed in an iron ball mill for 20 min with 280 rev/min clockwise and counterclockwise. The PIT wire was made by filling the powder mixture of Mg and B into Nb tube (outer diameter 4.5 mm / inner diameter 3.5 mm), rotary swaged to 4 mm diameter and inserted into Cu tube, before deforming to rectangular shape of approximately 1 × 1 mm^2. Afterwards the sample was heat

treated at 650°C for 30 min in Ar atmosphere. The cross section of the PIT wire is shown in Figure 10(a).

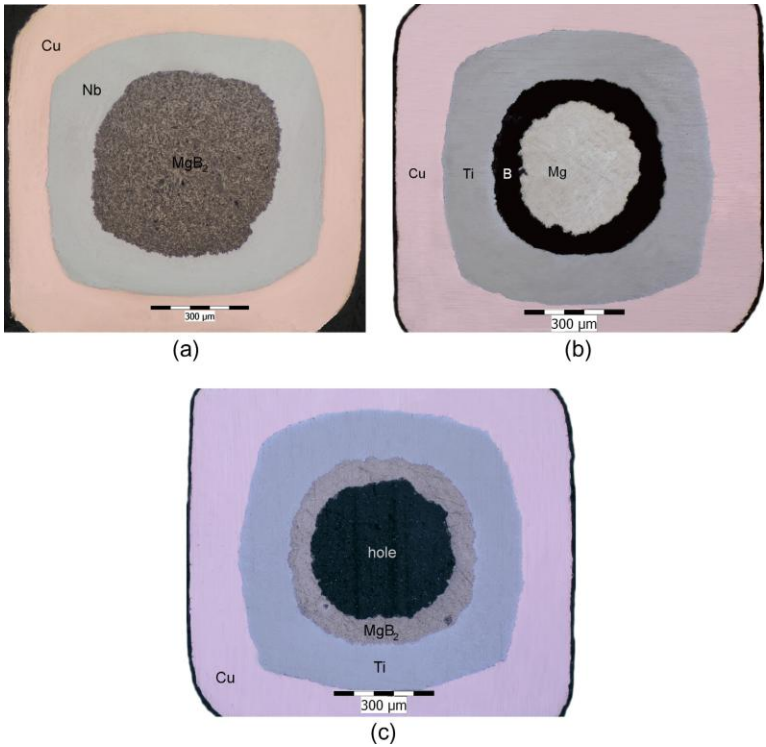

Figure 10 Micrographs of the cross section of the (a) PIT wire and of the IMD wire before (b) and after (c) annealing

For the fabrication of the IMD wire, a pure Mg rod with 3.5 mm diameter was placed at the center of a Ti tube (outer diameter 7 mm/inner diameter 5 mm) and the space between the Mg rod and the Ti tube was filled with a B powder (purity 99%, particles size ~200 nm). After initial rotary

swaging a Cu tube was added around the Ti tube and the composite was deformed to rectangular shape of approximately 1 × 1 mm^2. The IMD sample was then annealed at 640°C for 1 hour in Ar atmosphere. In Figure 10(b) and (c) cross sections of the IMD wire before and after annealing are shown, respectively. The B layer is changed to a new MgB_2 layer with a dense structure without visible porosity and a hole is created where the Mg core had been before heat treatment.

To determine what phases the MgB_2 cores are composed of, XRD analysis was performed. The measurement was done immediately after the preparation of powder samples in air atmosphere. The results are summarized in Table 1. Phase composition of the IMD and PIT wires measured by XRD is presented in wt%.

Table 1 Phase composition of IMD and PIT wires measured by XRD. The values are in wt%.

	MgB_2	MgO	Mg	Cu	Ti/Nb
IMD - wt%	93.5	3.5	2.2	-	0.8
PIT - wt %	87.0	8.0	1.3	1.1	2.6

The results show that greater phase purity and lower secondary phase amount was attained with the IMD sample. In the case of IMD wire the found Mg phase amount includes the rest of Mg on the inner side of superconducting layer in the central hole and corresponding MgO, because

Mg is known to have a large affinity to oxygen. The observed Cu, Ti and Nb amounts are due to the sheath materials that unintentionally got into powder samples.

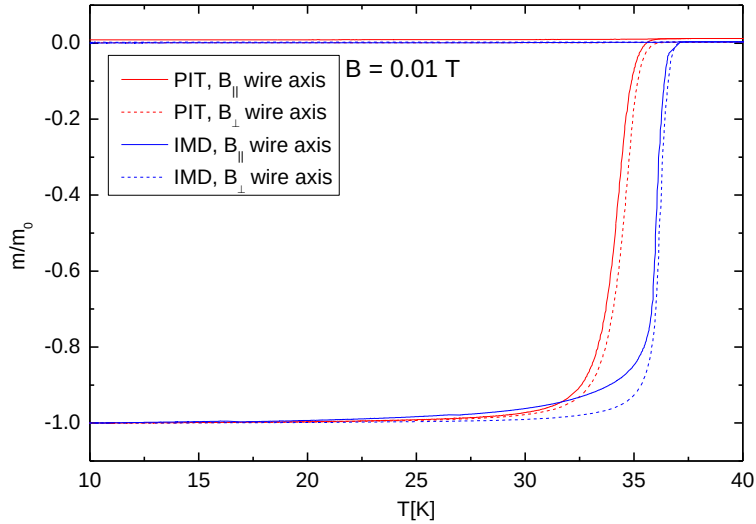

Figure 11 Zero field cooled and field cooled curves measured in applied field of 10 mT

Both wire samples have comparably high transition temperatures (Figure 11 and Table 2), with difference less than 0.6 K. For IMD sample T_c is slightly higher than for PIT sample and the transition of IMD is sharper than for PIT, see Table 2. These differences can be explained by improved phase purity in IMD wire due to reduced MgO phase introduced by Mg powder or Mg rod. Assuming that the same MgO layer is covering Mg particles and Mg rod,

considerably larger surface area of powder means larger amount of MgO. Very small difference was obtained for transition curves measured in parallel and perpendicular field orientation.

Table 2 Transition temperatures and transition widths

	T_c[K]	ΔT_c[K]
PIT	36.6	2.2
IMD	37.2	1.2

The measurements of the transport critical current density J_{ct} were made in magnetic field applied perpendicular to the wire axis ($B\perp$) up to 8 T in liquid helium at 4.2 K. Samples were 5 cm long with a gauge length of 5 mm. An electric field criterion of 1 μVcm^{-1} was used. The gauge length-sample length ratio was adequate to ensure complete current sharing into the MgB_2 layer/core. The insert was located in the bore of the superconducting magnet. J_{ct} of PIT wire was obtained by dividing the critical transport current, I_{ct}, with the area of the MgB_2 core. That of IMD wire was I_{ct} divided by the area of the annular MgB_2 layer. Figure 12 presents the magnetic and transport critical current density of the analysed wires.

From direct transport measurement higher J_{ct} values are found for IMD sample. At 8 T J_{ct} of IMD sample is almost by 90% higher than J_{ct} of PIT sample. Since there was a potential risk that IMD sample gets overheated and

quenches in low fields, its J_{ct}-characteristic was measured in a relatively narrow field range (6.5–8 T). In this range, both wires show practically the same field dependence-the ratios of the J_{ct}–values for IMD and PIT wire at 6.5 T and 8 T are equal (2.9 for the PIT wire, 3 for the IMD wire). At fields below 5 T J_{ct} of the PIT wire is stronger field-dependent.

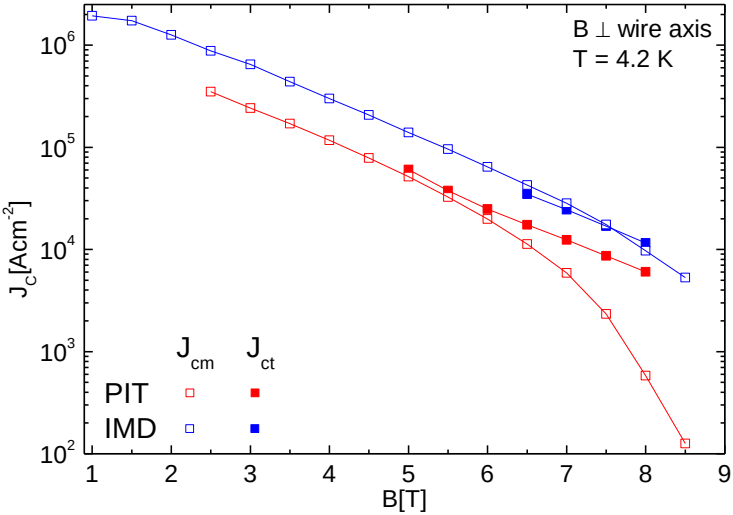

Figure 12 Comparison between the transport and magnetic critical current density of IMD and PIT wire

The mean effective activation energies of flux lines were calculated and their temperature dependence at 1 T and 3T is shown in Figure 13. The dependences are characterized by a dome-like shape, with maxima around T_{max}~15 K. With increasing field the maximum of $U(T)$-dependence shifts slightly to lower temperatures. The values of U are

much higher than found for classic high temperature superconductors measured under the same conditions. As expected U decreases with increasing applied field. Except for the case $B\|$ at 1 T U values are higher for IMD sample at T_{max}.

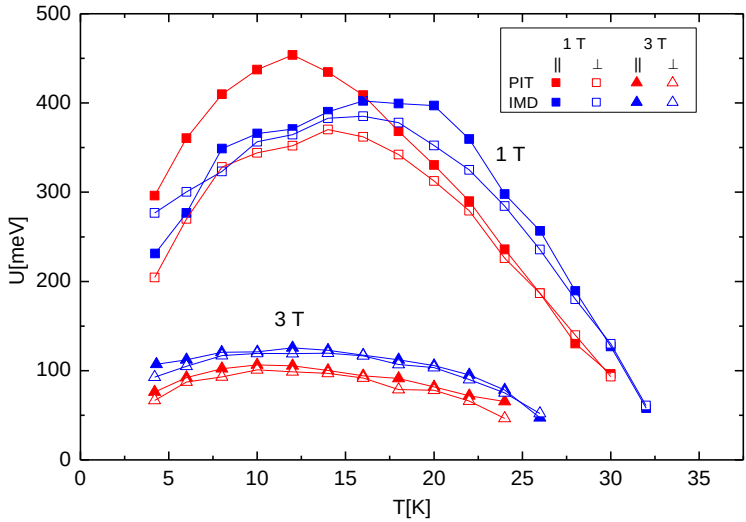

Figure 13 Mean effective activation energy of IMD and PIT sample

4.2 The pinning behaviour of a silver sheathed $Sr_{0.6}K_{0.4}Fe_2As_2$ pnictide superconductor

The Ag-sheathed $Sr_{0.6}K_{0.4}Fe_2As_2$ tape with Sn addition was produced by the ex-situ PIT process at IEE of Chinese Academy of Sciences. A mixture of a nominal Sr:K:Fe:As = 0.6:0.5:2:2.05 ratio was ball-milled under Ar atmosphere, packed into a Nb tubes and annealed at 900°C for 35 h. The thus obtained $Sr_{0.6}K_{0.4}Fe_2As_2$ precursor was

ground to powder in Ar atmosphere and mixed with 5 wt% Sn. Afterwards the powder was filled into a Ag tube with OD/ID of 8 mm/5 mm, respectively. After sealing, the tube was cold-worked by drawing and flat rolling to a tape with the superconductor cross-section area 0.1 × 4.3 mm^2. Finally, the tape was sintered at 850° C for 30 min.

Figure 14(a) shows J_c in both directions at selected temperatures. Higher J_c values are obtained when the field is applied perpendicular to the tape axis. The anisotropy ($J_c\perp/J_c\parallel$ ratio) is quite small (from 1.1 at 3 T to 1.3 at 12 T), and it vanishes with increasing temperature. At 10 T and 4.2 K, J_c values reach 4.5 × 10^4 Acm^{-2} and at 14 T, J_c is above 3.0 × 10^4 Acm^{-2}. Notably, up to 12 K, J_c values are still above 1.0 × 10^4 Acm^{-2} at 14 T. Concerning the field dependence of J_c, it decreases very slowly with increasing field. This is well visible if compared with J_c of a good MgB_2 wire (Figure 14(b)) [7]. Although J_c of MgB_2 is much higher in low fields, it drops rapidly and at 9 T and 4.2 K it becomes lower than 1000 Acm^{-2}. On the other hand, at 4.2 K and 10 K the Sr-122 sample exhibits very slow decrease of J_c, which starts from about 3 T.

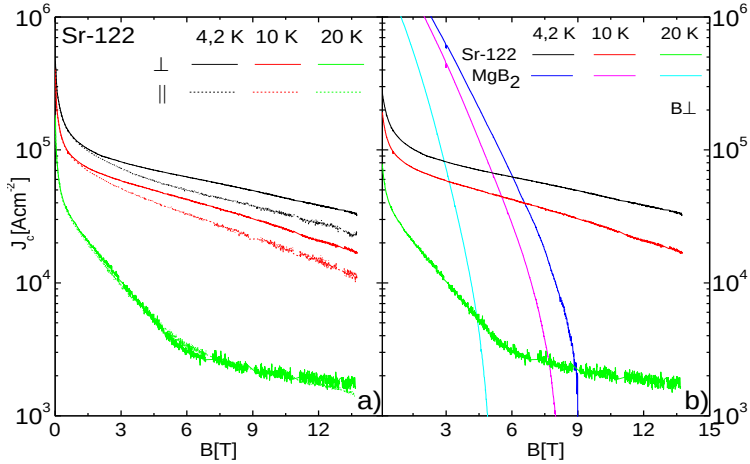

Figure 14 Magnetic field dependence of the critical current density J_c (a) and comparison (b) between Sr-122 and MgB_2 [7]. The applied fields up to 14 T were parallel (dashed line) and perpendicular (solid line) to the tape axis

The temperature dependence of the activation energy is plotted in

Figure 15(a) and (b) for both field directions. The first remarkable result is that the pinning energies could have been calculated in the fields as high as 13 T. However, even more interesting is the pinning behaviour as the field was increased. At 1 T the pinning energies reach their maximum values above 100 meV. As the field increases to 3 T or 5 T for $B\|$ and for $B\perp$, respectively, the activation energies become practically field-independent within measuring accuracy, in good agreement with the results for the critical current density. Upon initial decrease of J_c occurring up to 3 T or 5 T, J_c drops considerably slower.

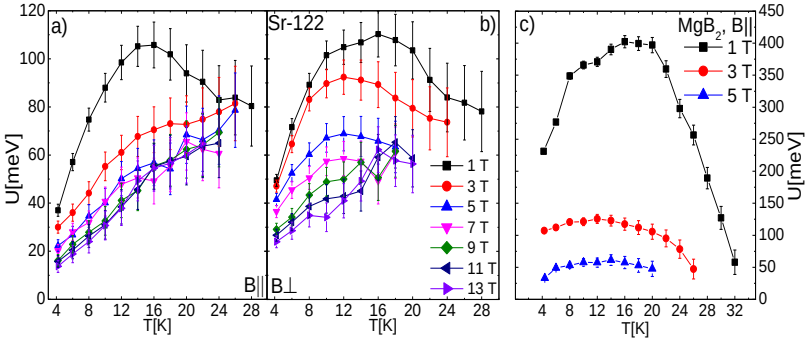

Figure 15 The temperature dependence of mean effective activation energy at various fields applied parallel (a) and perpendicular (b) to the tape axis. In (c) the $U(T)$ dependence is shown for MgB_2 at 1 T, 3 T and 5 T [7]

Figure 15(c) shows the $U(T)$-dependence of a MgB_2 wire at 1 T, 3 T and 5 T [7]. At 1 T the pinning energies are one order of magnitude higher than those of the Sr-122 tape. At 3 T the energies of the MgB_2 sample are still slightly higher and at 5 T they fall down to values comparable with the tape. Above 5 T the energies of the MgB_2 sample could not have determined at all. In addition, noticeable is the relatively swift decrease of MgB_2 pinning energies with increasing magnetic field in comparison with the tape.

4.3 MgB_2 wires prepared with various doping

Four series of single-core MgB_2 wires were manufactured each using a distinct amorphous boron nanopowder which was showered into the hole in Mg by vertical filling and densified by hand-pressing with a steel rod of appropriate

size. The hole had 2.4 mm in diameter and it was drilled in a pure Mg rod with 3.5 mm in diameter. As the sheath material, Nb tubes subjected to recrystallization annealing at 950°C/30 min with OD/ID of 5 mm/3.9 mm were used.

The first series was made with a special plasma-synthesized B powder [8] (made by the reduction of BCl_3 through hydrogen in a plasma torch) doped with carbon (Specialty Materials Inc., SMI+C powder, C concentration 4 at%, particle size 160 nm) and is referred to as SMI+C. For the second series, referred to as PVZ+C, the Pavezyum boron powder (purity>98.5%, particle size<250 nm) with somewhat lower C concentration of 2 at% was used. The last dopant were the SiO_2-nanoparticles (Sigma-Aldrich, particle size 10 nm, purity 99.5%, concentration 10 wt%), which were mixed with a pure amorphous boron powder (particle size ~200 nm) of purity 99% in a planetary ball mill for 10 minutes clockwise and counterclockwise. Wires formed using the SiO_2-nanoparticles are referred to as SiO_2. Finally, as a reference an undoped series, referred to as US, was made using the same starting boron powder with no additives (purity 99%) as was used for the SiO_2 series.
After packing the powder into Nb tubes in a glovebox under Ar atmosphere, the composites were rotary swaged to 4.5 mm in diameter and groove-rolled to dimensions about 1.5×1.5 mm^2. Eventually, the wires were cut to 5 cm pieces and every series was annealed for one hour in Ar at

temperatures 660°C, 650°C, 640°C, close to the melting point of Mg.

Figure 16 shows the cross-section micrographs of the SMI+C, PVZ+C and SiO_2-wire heat treated at 650°C for 1 hour. In Figure 16 (a) a large amount of unreacted Mg is visible. The shape of MgB_2 resembles annular layer arising in an ordinary IMD reaction. This became even more apparent in the SMI+C wire annealed at 640°C. On the other hand, the wire subjected to annealing at 660°C held less residual Mg and more MgB_2.

Figure 16 Optical micrographs of the cross-sections of the SMI+C wire (a), PVZ+C (b) and SiO_2 wire (c) heat treated at 650°C for 1 hour

Whereas there were lots of Mg remnants in the SMI+C wires, significantly smaller unreacted Mg amounts were

found in the PVZ+C wires with well-developed cylindrical cores, as can be seen in Figure 16 (b). Evidently, the used boron powder has a substantial effect on the diffusion reaction. In the wires made with SiO_2 addition, practically no unreacted Mg was observed (Figure 16 (c)).

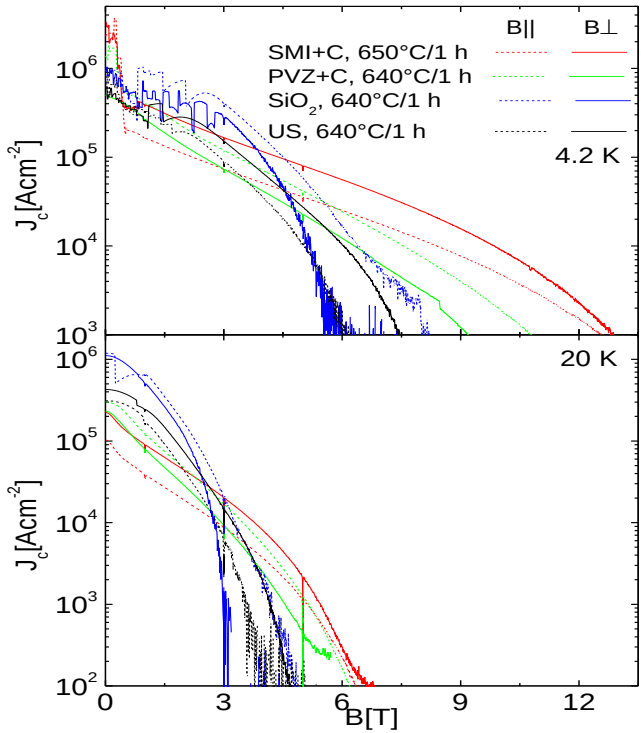

Figure 17 The field dependence of critical current density for the best wire of each series at 4.2 K and 20 K

The J_c-B dependences are plotted in Figure 17 for the best samples of each series at 4.2 K and 20 K. An excellent

J_c-performance exhibited the SMI+C series, with the highest critical current density of the wire annealed at 650°C/1 h. Compared to the corresponding reference sample, the current density of the SMI+C wire is higher from about 2.5 T with J_c at 4.2 K and 10 T almost 10000 Acm^{-2}, when the field was applied perpendicular to the wire axis. The same holds for the parallel field direction. J_c of the SMI+C wire exceeds that of the undoped wire at 3 T. The J_c values in the perpendicular direction are roughly twice as high as those in the parallel applied field within most of the measuring interval. The second best wire of the SMI+C series was that sintered at 640°C/1 h with 10000 Acm^{-2} at 9 T.

On the other hand, higher J_c values were found in the parallel direction for the PVZ+C wires. The wire annealed at 640°C/1 h showed the highest critical current density of the series, reaching 10000 Acm^{-2} at 7.5 T and 4.2 K. The J_c anisotropy ($J_c\|$ to $J_c\perp$ ratio) of the PVZ+C series ranges from 1.58 at low fields to 2.37 at higher fields. The second best J_c -performance showed the wire heat-treated at 650°C/1 h.

4.4 Effect of Dy_2O_3 doping on phase formation and properties of MgB_2 wires produced by MIMD

MgB_2 wires were made by the MIMD process, starting with a Mg rod (3.5 mm diameter) placed coaxially in a Nb tube (outer/inner diameter 5.2/3.6 mm). The Nb tube with the Mg

rod inside was rotary swaged to 4.8 mm diameter to make sure the rod is held firmly in position. The rod was subsequently drilled and the hole (2.4 mm diameter) was filled with the same carbon predoped boron powder (Specialty Materials Inc., C concentration 4 at%, particle size 160 nm) as used in the previous chapter, however, this time with addition of 2 wt% or 3 wt% Dy_2O_3 nanopowder (Sigma-Aldrich, purity 99.9%, particle size 100 nm). Before filling the powder mixture (boron + Dy_2O_3) was homogenized by ball-milling at 150 revs/min for 10 minutes. The powder filled into the hole in Mg was densified by handpressing with a steel rod of appropriate size and by rotary swaging of the composite to 4.2 mm diameter. The composites were then groove-rolled to wires with approximately 1.5 × 1.5 mm^2 and finally heat-treated at 650°C/1 hour, 650°C/4 hours and 675°C/4 hours in Ar atmosphere. For comparison, the results for a reference

Table 3 Doping levels and heat treatment conditions of wires

sample name	Dy_2O_3 (wt%)	heat treatment
REF	0	650°C/1 h
D1	2	650°C/1 h
D2	2	650°C/4 h
D3	2	675°C/4 h
D4	3	650°C/1 h
D5	3	650°C/4 h
D6	3	675°C/4 h

sample free of Dy_2O_3, whose preparation details are described in section 4.3, are used. Table 3 lists the Dy_2O_3 doping level and heat treatment conditions.

Figure 18 demonstrates the effect of Dy_2O_3 doping on the reactivity of C-predoped B powder observed by optical microscope in wires heat-treated (HT) at 650°C for one hour. It is evident that Dy_2O_3 doping promotes Mg diffusion into B. In the wire made without Dy_2O_3 addition a discontinuous annular-like MgB_2 layer resembling traditional IMD wires with lots of unreacted Mg can be seen while in the wires with Dy_2O_3 a more uniform and denser MgB_2 structure, though still annular, with no large cracks across the layer is observed.

Even though the qualitative difference between the wires without and with Dy_2O_3 sintered at the Mg melting point (650°C) for one hour is apparent, the doping itself is not sufficient for perfect diffusion reaction between Mg and B, leaving remnants of Mg and B on the outer and inner side of MgB_2 layer, respectively. Further enhancement of boron powder reactivity was attained by applying higher HT temperature and longer HT time.

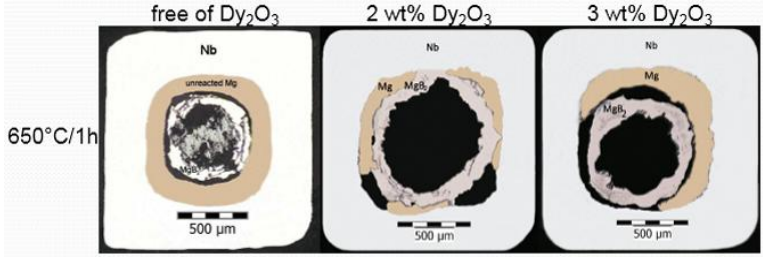

Figure 18 Cross sections of the wires heat-treated at 650°C for 1 hour without and with Dy_2O_3 addition

Figure 19 compares cross-sections of the wires doped with 2 wt% or 3 wt% Dy_2O_3 heat-treated at 650°C/1 hour, 650°C/4 hours and 675°C/4 hours. Longer HT time or a combination of longer HT time and higher HT temperature brings about major improvement of C-doped B powder reactivity and proves to be very beneficial for MgB_2 formation. The cross sections of the wires heat-treated at 650°C/4 hours and 675°C/4 hours show fully reacted MgB_2 structure with practically no residual Mg visible.

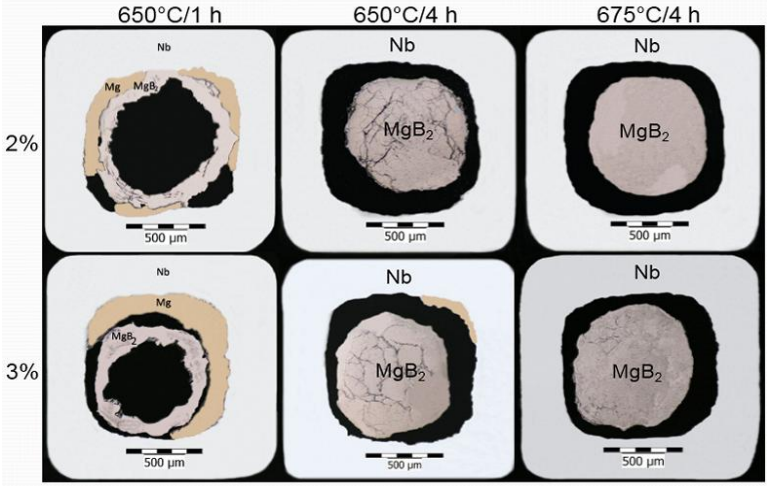

Figure 19 Optical micrographs of cross sections of the wires doped with Dy_2O_3 heat-treated at 650°C/1 hour, 650°C/4 hours and 675°C/4 hours

Figure 20(a) and (b) shows the in-field critical current densities J_c of the wires with 2 wt% or 3 wt% Dy_2O_3 for $B\perp$ at 4.2 K and 20 K. The effects of HT and Dy_2O_3 concentration are distinctly visible in the $J_c(B)$-characteristics. While the values of J_c are strongly affected by HT, they vary only weakly with Dy_2O_3 concentration. For both concentrations, J_c rises with increasing HT temperature and longer HT period. Highest J_c was attained for samples D3 and D6 with more than 10^6 Acm^{-2} at 1 T and 4.2 K. Owing to weaker field dependence of samples D2 and D5 allowing better performance in high field region, their J_c is higher above 8 T in comparison with D3 and D6 at 4.2 K.

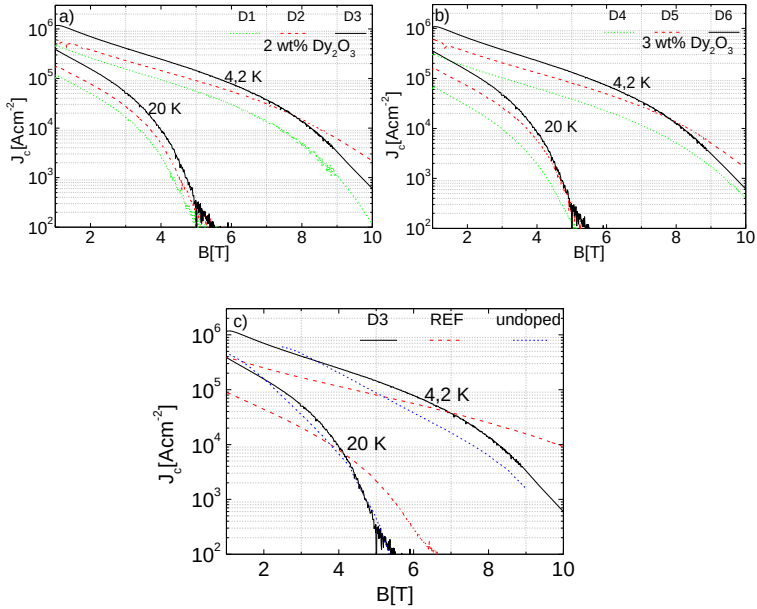

Figure 20 The critical current densities of the wires with 2 wt% (a) or 3 wt% (b) Dy_2O_3 and comparison (c) of J_c with a Dy_2O_3-free sample and an undoped sample (all for $B\perp$)

Figure 20(c) compares J_c of sample D3, a Dy_2O_3-free reference sample and an undoped sample prepared using a pure boron powder (no carbon) [9], demonstrating the high quality of D3. One can see that D3 performs better than the other two samples within most of the measured field range. At 4.2 K, J_c of D3 surpasses that of the Dy_2O_3-free sample in the fields up to 7 T, with the same trend holding up to 4 T at 20 K. Concerning the undoped sample, its J_c is lower than J_c of D3 in the whole field range except for a narrow low-field region (2.5 T-3 T and 1 T-2 T at 4.2 K and 20 K,

respectively), in which their critical current density is comparable.

4.5 Enhanced J_c of MgB_2 wires doped with $BaZrO_3$

Besides SiO_2 nanoparticles, which have not proved to be beneficial for the properties of MgB_2 wires, $BaZrO_3$ nanopowder is another previously untested additive whose effects on superconductivity in MgB_2 were explored within the scope of this thesis. For the experiment, minute amounts of the substance were mixed into pure boron precursor powder. The thus produced wires exhibited very good phase purity, sharp transition with high critical temperature (close to 39 K) and enhanced J_c with the highest value of almost 2 MA/cm^2 at 4.2 K and 2 T. These results demonstrate excellent qualities of wires doped with $BaZrO_3$ nanopowder made by MIMD method.

A series of single-core MgB_2 wires was produced by the MIMD process. Nb tubes (outer/inner diameter 5.2/3.6 mm) subjected to recrystallization annealing at 950°C/30 minutes were used as the sheath material. In Nb tube a pure Mg rod of 3.5 mm in diameter was inserted and the tube was rotary swaged to 4.8 mm in diameter to ensure the rod is firmly fixed in position and does not move when drilled. For drilling a 2.4 mm bit was used and the hole was filled with a boron powder doped with $BaZrO_3$ nanoparticles. Before filling the amorphous boron powder (particle size ~200

nm) of purity 99% was mixed with $BaZrO_3$ nanopowder (average particle size of 15 nm, 95% purity with about 5% ZrO_2) and the mixture was homogeneized in a planetary ball mill for 10 minutes clockwise and counterclockwise at 150 revs/min. In order to densify the powder, it was continually pressed with a steel rod of appropriate size during filling. Subsequently, the filled tubes were further densified by rotary swaging to 4.2 mm diameter. The composites were then groove-rolled to wires with approximately 1.5×1.5 mm^2 and finally heat-treated at 640°, 650°C and 660°C for one hour in Ar atmosphere. As a reference sample, an undoped wire studied in [9] was used for comparison. Table 4 lists the $BaZrO_3$ doping level and heat treatment conditions.

Table 4 Doping levels and heat treatment conditions of wires

sample	Dy_2O_3 (wt%)	heat treatment
REF	0	660°C/1 h
B1	2	640°C/1 h
B2	2	650°C/1 h
B3	2	660°C/1 h
B4	5	640°C/1 h
B5	5	650°C/1 h
B6	5	660°C/1 h

XRD analysis was carried out on crushed MgB_2 cores extracted from Nb sheaths. As can be seen in Table 5 summarizing the results all samples exhibit excellent MgB_2

phase purity with only little secondary phases varying very weakly with doping and heat treatment conditions. The amount of MgO contained in $BaZrO_3$ doped MIMD-processed MgB_2 wires is lower or comparable with that found in an undoped IMD wire presented in section 4.1. Besides MgO, BaB_6 was also observed in the MgB_2 cores due to Ba reaction with B. It indicates that $BaZrO_3$ dopant decomposed during heat-treatment. No Zr-containing compound was detected by XRD probably due to its microstructure-nanoscale grain size and/or amorphous phase. An interesting result is that there was no residual Mg detected by XRD underlining good phase purity of the samples.

Table 5 Phase composition of the $BaZrO_3$ doped samples obtained from XRD analysis

sample	MgB_2 [%]	MgO [%]	BaB_6 [%]
B1	96	2,5	1,5
B2	96	2,3	1,7
B3	96	2,4	1,6
B4	93	3,5	3,5
B5	93	4	3
B6	93	4	3

The in-field critical current density J_c of the wires with 2 wt% or 5 wt% $BaZrO_3$ for both field directions at 4.2 K and 20 K is shown in Figure 21(a) and Figure 21(b). The best $J_c(B)$-characteristics were obtained for the wires heat-treated at 640°C. From the perspective of dopant

concentration, more dopant acted positively on the critical current density leading to the highest J_c value for sample B4 with 2 MAcm^{-2} at 4.2 K and 2 T. The anisotropy of the wires rises with increasing sintering temperature and dopant concentration, but the reason for J_c anisotropy is not yet understood. Within most of the field range higher J_c was obtained for $B\|$. The same trends hold at 4.2 K as well as at 20 K.

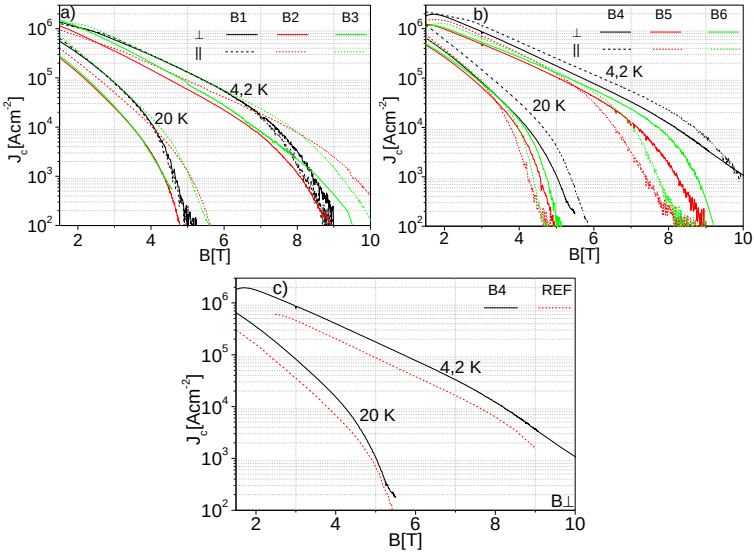

Figure 21 The critical current densities of the wires doped with 2 wt% (a) or 5 wt% (b) $BaZrO_3$ and comparison (c) of J_c with a $BaZrO_3$-free sample

In Figure 21(c) $J_c(B)$-dependences are shown for the best doped sample B4 and for an undoped reference sample [9]. Evidently, the use of $BaZrO_3$ brought about an improvement. B4 outperforms the reference sample in the

whole field range at both temperatures and, moreover, the reference sample exhibits a wide flux jump region with flux jumps occurring up to 2.5 T (flux jumps cut out in the figure), while for B4 flux jumps vanished above 1.5 T.

5 Conclusions

The dissertation thesis aims to gain a thorough understanding of how the microstructure, superconducting properties and their interplay in MgB_2 are connected with the production process. For this purpose, several series of MgB_2 wires processed under varying conditions were investigated in detail.

First, mono-core MgB_2 wires produced by internal magnesium diffusion process and in-situ powder-in-tube technique were studied and compared. It has been shown that IMD process results in a core with significantly increased density of active superconducting MgB_2 layer and low secondary phases content. This quality came through in the critical current density J_c of the wires. The thick low porosity superconductor coming from the diffusion reaction outperforms the PIT-processed superconductor in the whole measured field range. For demonstration, IMD wire attains a critical current density of 10^4 Acm^{-2} at 4.2 K and 8 T while PIT wire at 4.2 K and 6.5 T. The comparison of J_c values at 4.2 K and 8 T shows that the sample prepared by IMD process has up to 50 times higher J_c than PIT sample. At 20

K this difference gets smaller, J_c of IMD sample is higher by one order of magnitude.

Second, in order to be able to judge the qualities of MgB_2 from a broader perspective, one chapter of the thesis is dedicated to a different kind of superconductors-iron-containing pnictides, particularly Sr-122 tape. The investigated Ag-sheathed $Sr_{0.6}K_{0.4}Fe_2As_2$ tape exhibited excellent J_c performance in high magnetic fields. In low fields, a decline in J_c with increasing field was observed just as was in MgB_2, although at a significantly lower absolute value. A kink-like crossover to a much flatter in-field J_c-dependence at higher fields allows for a much better high field performance than that of MgB_2. This kink is reflected in and may be attributed to the field dependence of the mean effective activation energy U obtained from magnetic relaxation measurements. Therefore, in comparison with pnictides, MgB_2 is appropriate for operating especially in lower magnetic fields.

Third, the effects of different boron powders on wire properties were studied. Plus, a new type of dopant, the SiO_2 nanoparticles, not tested as MgB_2 additive so far, was used. It was found that doping of boron powder has a substantial effect on the diffusion reaction and that carbon acts as a MgB_2 growth suppressor. The highest J_c exhibited a sample prepared using a carbon containing (4 at%) boron powder heat-treated at 650 °C/1 h, with almost 10000 Acm^{-2} at 10 T

and 4.2 K. At the same time, the best sample from the point of view of J_c showed the lowest pinning energies, indicating that high J_c is due to an increased number of pinning sites. Concerning the SiO_2-doped samples, they exhibited a wide flux jump region in their hysteresis loops and a quickly declining field dependence of J_c. Hence, SiO_2 nanopowder has not proved to have a beneficial effect on MgB_2.

Fourth, it was attempted to compensate the detrimental effect of carbon doping on boron powder reactivity by adding minute amount of Dy_2O_3 nanopowder to the boron and by sintering the composites at increased temperature for longer time. The reactivity of the boron powder was enhanced by Dy_2O_3 addition, however, in order to achieve fully reacted MgB_2 core in the wires, higher HT temperature or longer HT period must have been applied. Concerning the MgB_2 phase purity, Dy_2O_3 was beneficial for superconductor formation coming from the diffusion reaction with the highest MgB_2 content about 90%. The superconducting properties were found to be affected mainly by the heat treatment conditions rather than by the Dy_2O_3 addition with the highest critical current density of 10^6 Acm^{-2} at 4.2 K and 1 T measured for a wire sintered at 675°C/4 hours. This is reflected in the observed values of the mean effective activation energies of flux lines, which were the highest for the same wire.

Fifth, besides SiO_2, $BaZrO_3$ nanopowder is another previously unexplored additive whose effects on superconductivity in MgB_2 were studied within the scope of the thesis. The dopant turned out to be very beneficial for MgB_2. It did not worsen the boron powder reactivity at all. The wires exhibited very good phase purity, sharp superconducting transition with high critical temperature (close to 39 K) unaffected by the dopant and enhanced J_c with the highest value of almost 2 MA/cm^2 at 4.2 K and 2 T. These results demonstrate excellent qualities of wires doped with $BaZrO_3$ nanopowder made by the modified internal magnesium diffusion method.

Bibliography

[1] B. Brunner, A. Windbichler, M. Reissner, P. Kováč, I. Hušek J., *J. Supercond. Novel. Magn.*, vol. 28, p. 443, 2015.

[2] B. A. Glowacki, M. Majoros, M. Vickers, J. E. Evetts, Y. Shi, I. McDougall, *Supercond. Sci. Technol.*, vol. 14, p. 193, 2001.

[3] P. Kováč, I. Hušek , T. Melišek , J. C. Grivel, W. Pachla, V. Štrbík, R. Diduszko , J. , *Supercond. Sci. Technol.*, vol. 17, p. L41, 2004.

[4] H. Suo, C. Beneduce, M. Dhallé, N. Musolino, Jean-Yves Genoud, René Flükiger, *Appl. Phys. Lett.*, vol. 14, p. 193, 2001.

[5] G. Giunchi, S. Ceresara,G. Ripamonti, A. Di Zenobio, S. Rossi, S. Chiarelli, M. Spadoni, , *Supercond. Sci. Technol.*, vol. 16, p. 285, 2003.

[6] Anderson P. W., *Phys. Rev. Lett.*, vol. 9, p. 309, 1962.

[7] Brunner B., Kováč P., Reissner M., Hušek I., Melišek T., Pardo E., *Physica C*, vol. 515, p. 39, 2014.

[8] Ye S., Song M., Matsumoto A., Togano K., Takeguchi M., Ohmura T., Kumakura H., *Supercond. Sci. Technol.*, vol. 26, p. 125003, 2013.

[9] Kulich M., Kováč P., Hain M., Rosová A., Dobročka E., *Supercond. Sci. Technol.*, vol. 29, p. 035004, 2016.